




Article

A Novel IoT-Enabled Healthcare Monitoring Framework and Improved Grey Wolf Optimization Algorithm-Based Deep Convolution Neural Network Model for Early Diagnosis of Lung Cancer

Reyazur Rashid Irshad ¹, Shahid Hussain ², Shahab Saquib Sohail ^{3,*}, Abu Sarwar Zamani ⁴,
Dag Øivind Madsen ^{5,*}, Ahmed Abdu Alattab ^{1,6}, Abdallah Ahmed Alzupair Ahmed ¹,
Khalid Ahmed Abdallah Norain ¹ and Omar Ali Saleh Alsaiani ¹

¹ Department of Computer Science, College of Science and Arts, Najran University, Sharurah 68341, Saudi Arabia

² Department of Computer Science and Engineering, Sejong University, Seoul 30019, Republic of Korea

³ Department of Computer Science and Engineering, School of Engineering Sciences and Technology, Jamia Hamdard, New Delhi 110062, India

⁴ Department of Computer and Self Development, Preparatory Year Deanship, Prince Sattam bin Abdulaziz University, Al-Kharj 11942, Saudi Arabia

⁵ USN School of Business, University of South-Eastern Norway, 3511 Hønefoss, Norway

⁶ Department of Computer Science, Faculty of Computer Science and Information Systems, Tamar University, Tamar 87246, Yemen

* Correspondence: shahabssohail@jamiahamdard.ac.in (S.S.S.); dag.oivind.madsen@usn.no (D.Ø.M.)



Citation: Irshad, R.R.; Hussain, S.; Sohail, S.S.; Zamani, A.S.; Madsen, D.Ø.; Alattab, A.A.; Ahmed, A.A.A.; Norain, K.A.A.; Alsaiani, O.A.S. A Novel IoT-Enabled Healthcare Monitoring Framework and Improved Grey Wolf Optimization Algorithm-Based Deep Convolution Neural Network Model for Early Diagnosis of Lung Cancer. *Sensors* **2023**, *23*, 2932. <https://doi.org/10.3390/s23062932>

Academic Editor: JeongGil Ko

Received: 8 February 2023

Revised: 2 March 2023

Accepted: 3 March 2023

Published: 8 March 2023



Copyright: © 2023 by the authors. Licensee MDPI, Basel, Switzerland. This article is an open access article distributed under the terms and conditions of the Creative Commons Attribution (CC BY) license (<https://creativecommons.org/licenses/by/4.0/>).

Abstract: Lung cancer is a high-risk disease that causes mortality worldwide; nevertheless, lung nodules are the main manifestation that can help to diagnose lung cancer at an early stage, lowering the workload of radiologists and boosting the rate of diagnosis. Artificial intelligence-based neural networks are promising technologies for automatically detecting lung nodules employing patient monitoring data acquired from sensor technology through an Internet-of-Things (IoT)-based patient monitoring system. However, the standard neural networks rely on manually acquired features, which reduces the effectiveness of detection. In this paper, we provide a novel IoT-enabled healthcare monitoring platform and an improved grey-wolf optimization (IGWO)-based deep convolution neural network (DCNN) model for lung cancer detection. The Tasmanian Devil Optimization (TDO) algorithm is utilized to select the most pertinent features for diagnosing lung nodules, and the convergence rate of the standard grey wolf optimization (GWO) algorithm is modified, resulting in an improved GWO algorithm. Consequently, an IGWO-based DCNN is trained on the optimal features obtained from the IoT platform, and the findings are saved in the cloud for the doctor's judgment. The model is built on an Android platform with DCNN-enabled Python libraries, and the findings are evaluated against cutting-edge lung cancer detection models.

Keywords: Internet-of-Things; healthcare monitoring; lung cancer; tasmanian devil optimization; improved grey wolf optimization; deep convolutional neural network

1. Introduction

Lung cancer is one of the most common diseases in the world, accounting for 1.3 million diagnoses and 1.2 million deaths per year [1]. The most prevalent lung disorders have been lung cancer, asthma, pneumonia, and pulmonary edema. The respiratory illnesses include lung circulation, tissue disorders, and airway disorders, with asthma being a specific chronic lung disease that worsens the lung's breathing difficulties [2]. Bronchitis, pneumonia, and bronchiolitis are the three forms of lung infection caused by bacteria and viruses that seriously infect the lungs. They are all harmful to the lungs and can be life-threatening.

It permits the oxygen to deliver carbon dioxide, while the humidity level and temperature allow the waste gases to be removed. Incurable lung disorders worsen breathing conditions and leave scars on the body, reducing people's life expectancy by 25% in five years. The primary activities of the respiratory system are protection, gas exchange, air movement, and sound generation, with the avoidance of lung illnesses and other physical treatments being one of the most important needs for a longer life [3].

Since lung cancer patients do not have symptoms until the disease has advanced to an inoperable level, their chance of survival is just about 15%, even with therapy; however, if diagnosed early, the treatment is highly effective, improving the survival rate by up to 67% [4]. Consequently, one of the main challenges is to come up with strategies that aid in early lung cancer diagnosis and thereby enhance the healthcare system for lung cancer patients [5]. Several procedures, such as chest radiography, sputum cytology, light-induced fluorescence endoscopy, and serum biomarkers, are being used to identify lung cancer, however, none of these have been demonstrated to be effective in accurately diagnosing the disease. Serum tumor indicators on pathological types, staging, monitoring, and prognostication of lung cancer [6] with serum squamous cell carcinoma antigen (SCC) [7], carcinoembryonic antigen (CEA) [8], and neuron-specific enolase (NSE) [9] are regarded to be successful strategies for lung cancer detection; nevertheless, these are laborious techniques [10]. Recent advances in artificial intelligence technology, on the other hand, have resulted in strong neural network models that resemble the human brain system and have shown the ability to anticipate a very complicated system with high accuracy, with little effort and time [11]. On the other hand, the proliferation of sensing technology through the Internet-of-Things (IoT) platform represents sensible objects such as processing capabilities, locating systems, programs, and other devices that sense and acquire data for various reasons [12].

There are three categories of IoT [13]: industrial, consumer, and enterprise IoT, where the manufacturing process is enhanced to employ selections and devices. It links a wide range of products to exchange and link data with smartphones, appliances, and wearables devices. It serves the demands of the consumer and expands the network of interconnected devices, including those connected to thermostats, vehicles, appliances, and homes. The IoT includes devices such as wearables, security systems, trackers, and door locks that capture and exchange data (e.g., temperature, pressure, motion, and light, etc.) to interact with other information across sensors, bridges that perform specifications, activation, security, communication, and detecting activities. It uses sensors to perceive multiple objectives in several domains and has proven efficient in production, agility, mobility, security, and healthcare systems with low costs. The performance of the IoT system is, however, hindered by several limitations, including connectivity challenges, integration issues, complexity, security concerns, privacy concerns, and noisy data [14].

Primary, secondary, and territorial healthcare systems [15] assist people by providing care and sickness prevention. The emergence of IoT technologies enables wearable devices to monitor patients, which are used to diagnose sickness and chronic diseases, thereby improving people's health and viability, resulting in smart healthcare [16]. The advantages of smart healthcare, which monitors, analyzes, and records health information, include education, immunization, child healthcare, and nutrition. The benefits of smart healthcare services, therefore, include healthcare prevention, rehabilitation, promotion, treatment, and diagnostics. All sensors and devices are connected to specialized devices that communicate with the patient's body via smart sensors and connected devices. It analyzes the state of healthcare records and provides the information needed to follow patients and their healthcare and access their medical records. The software packages are utilized to get healthcare feedback, knowledge-based decision support, and data from the patient's respiratory system. Their details are then saved in a database for future planning and training to encapsulate the desired healthcare through healthcare applications. Consequently, it enhances integrated medical care with patient mobility, improved treatment, and cost savings. However, one of the most challenging tasks is acquiring data and identifying the most

important attributes, as intimately linked data and its features play a vital role in enhancing the accuracy and sensitivity of these models [17]. In this paper, we developed a novel IoT-enabled healthcare monitoring platform and a grey-world optimization-based deep convolution neural network model with optimal feature selection based on the Tasmanian Devil Optimization algorithm to aid in lung cancer identification. Our contribution is threefold, as detailed below.

1. We developed an IoT platform, inferred the mechanism for acquiring lung disease data, and investigated the process for extracting the most significant attributes employing the Tasmanian Devil Optimization (TDO) algorithm, which enables high accuracy in the diagnosis of lung cancer.
2. We investigate the mechanism of the Grey-Wolf Optimization algorithm and modify its convergence rates, resulting in an improved GWO algorithm that is employed to fine-tune the parameters of the deep convolutional neural network model. Eventually, we presented an IoT-enabled platform with an IGWO-based DCNN model for lung cancer detection.
3. The developed model was trained and tested on the benchmark Exasens dataset, and its accuracy, sensitivity, specificity, and precision were evaluated against state-of-the-art clinical decision support systems (CDSS), regional-based convolutional neural networks (RCNN), active contour method (ACM), and Mask Region-Convolutional Neural Networks (Mask R-CNN) models for lung cancer detection.

The remainder of the article is organized as follows: Section 2 describes the related works. The suggested framework is designed in Section 3, and the experimental findings are discussed in Section 4. Section 5 concludes the article.

2. Literature Survey

Almezhghwi et al. [18] introduced a support vector machine, Alex Net, and VGG-16-based deep learning models for image classification of chest X-rays. Their research shows that the first method (Support vector machine) accurately predicts the classification of X-ray image data, while the second and third methods estimate the classification and features of skin lesions. This implies that the multi-class support vector machine uses twelve throat disorders for feature classification, with a robust, rapid, and easy prediction of lung disease.

A novel medical prediagnostic approach combining deep learning and fine-tuning has been shown by Han et al. [19]. Hemorrhagic stroke and lung images are segmented and categorized for classification reasons. The segmentation process classifies the actual images based on the network object of the image. The performance of the suggested approach is measured in terms of accuracy, speed, and efficiency. As a result, several aspects of diseases in the health-of-things domain are examined to refine the classification and segmentation process.

A clinical decision support system (CDSS) was developed by Rehm et al. [20] to identify patient ventilation management in the critical care unit. The IoT device used to transmit and store data from numerous devices and ventilators is monitored by the critical care unit. The development of a machine learning classifier leverages an acute respiratory distress syndrome (ARDS) to anticipate the condition. It improves illness identification, management, and diagnosis. The analyzed scalability problems are optimized, though.

Ahmed et al. [21] used a regional-based convolutional neural network (RCNN) in an IoT-based framework to detect COVID-19. In their model, a deep learning architecture was used to assist COVID-19 identification from samples of chest X-rays amplified by sensors, while the model of the Region Proposal Network (RPN) is used for executing regions and proposals. Distinct datasets are investigated and assessed using a varied learning technique, resulting in accurate and perfect case recognition; as a consequence, diverse images are anticipated for different architectures.

Ma et al. [22] introduced length-of-stay (LOS) to assess paediatric and respiratory disorders using the decision tree method. In their approach, the two techniques of expansion and computation turn dates, texts, and numbers into numeric data from a wide

range of data types. Following that, the data is analyzed to construct and test the decision tree algorithms. It accurately classified different ailments while cutting healthcare costs. Therefore, they used multi-class-based classification algorithms to categorize the diseases.

A fully automated approach based on the health of things was demonstrated by Xu et al. [23] to classify CT images. In their model, a two-step technique is employed to classify and segment CT (computed tomography) images, and so the images are classified by 14 models in the first stage by segmenting the lesion into 8 models to discover the existent regions. The image classification approach outperforms in terms of being more precise, reliable, and effective.

To segment CT images of the lungs, Skourt et al. [24] developed a deep learning-based method. In this approach, the segmentation process classifies the image to recover and extract the segmented maps, while the pooling and up-sampling are the two layers used to minimize the spatial dimension of encoder and decoder objects. Although diverse segmentation tasks are conducted in wide regions, they have not explored the classification of lung cancer.

In contrast to the typical method, which complements existing training data to identify the region of lung segments, Medeiros et al. [25] suggested an Active Contour Method (ACM) approach for lung segmentation. In their method, the margins of pulmonary regions increase the fuzzy border detector to better curve adaption, thereby accelerating the region to initialize the lung segments. Although the model appears to perform fast, precisely, and sensitively at the selected level, the system lack to support the real-time diagnostic systems.

Cai et al. [26] devised a Mask Region-Convolutional Neural Network (Mask R-CNN) and ray-casting volume rendering algorithm to undertake the 3D modules of the pulmonary nodule. Their proposed method, which comprises multiple modules such as pre-processing, segmentation, and three-dimensional, was capable of detecting other diseases and improving the segmentation network. The findings demonstrate the applicability of a multi-view technique for various parameters, allowing for more exact segmentation and detection of the pulmonary nodules. Table 1 tabulated the literature survey.

Table 1. Literature Survey.

| Author | Methods | Advantages | Limitations |
|------------------------|---|--|--|
| Almezhghwi et al. [18] | support vector machine, Alex Net, and VGG-16-based deep learning models | A robust, rapid, and easy prediction of lung disease | Minimum scalability |
| Han et al. [19] | Medical prediagnostic approach | Higher accuracy, speed, and efficiency | Less aspect of health-of-things domain |
| Ahmed et al. [21] | RCNN | Resulting in accurate and perfect case recognition | Computational; difficulties |
| Ma et al. [22] | Length-of-stay (LOS) | Accurately classified different ailments | Huge cost |
| Xu et al. [23] | A fully automated approach | More precise, reliable, and effective | Not suitable for big dataset |
| Skourt et al. [24] | Deep learning | Minimize the spatial dimension of encoder and decoder objects | Not explored the classification of lung cancer |
| Medeiros et al. [25] | Active Contour Method (ACM) approach | Perform fast, precisely, and sensitively | System lack to support the real-time diagnostic systems. |
| Cai et al. [26] | Mask R-CNN | Capable of detecting other diseases and improving the segmentation network | Higher time taken for execution |

3. The Proposed IoT-Enabled Platform with IGWO-Based DCNN Model

The deep CNN accomplishes lung disease classification employing both the training and testing mechanisms, as shown in the block diagram in Figure 1. The figure depicts the IoT body sensor devices that collect each patient's health data and identify lung cancer using the proposed IoT-enabled IGWO-based DCNN model representing a detailed healthcare monitoring system, and is explained in the following sub-section.

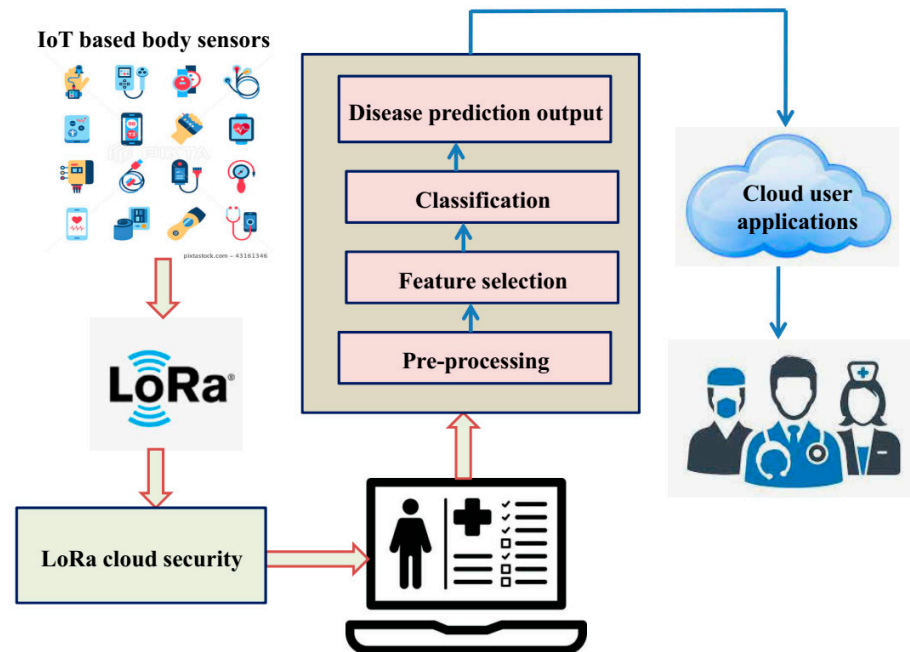


Figure 1. The schematic diagram with workflow of the proposed IoT enabled grey-wolf optimization-based deep convolution neural network (IGWO-based DCNN) model.

3.1. Pre-Processing

Pre-processing is important in rationalizing the data for effective algorithm use and thus helps to clean the dataset by removing redundancies and dealing with missing values. Consequently, we verified the patient's blood pressure, cholesterol levels, and age groups, and replaced the missing attribute with specified values [27], such that the values are substituted in the same position for the matched attributes [28]. Furthermore, the patient's health concerns are classified into distinct groups based on the type of lung pain.

3.2. Feature Selection

Considering the Tasmanian devil hunting behaviour patterns, it presents two sources of food, feeding on carrion and hunting and nourish on prey [29], which is employed to accomplish the optimal control, enabling the Tasmanian Devil Optimization (TDO) algorithm to acquire the important features that are closely related to lung cancer diagnosis. The features' optimal control mechanism imitates the Tasmanian devil's algorithm search and attempts to locate the most suitable food sources as given by Equation (1).

$$MA = \begin{bmatrix} MA_1 \\ \vdots \\ MA_j \\ \vdots \\ MA_X \end{bmatrix}_{X \times Y} = \begin{bmatrix} ma_{1,1} & \cdots & ma_{1,k} & \cdots & ma_{1,y} \\ \vdots & \ddots & \vdots & \ddots & \vdots \\ ma_{1,1} & \cdots & ma_{j,k} & \cdots & ma_{j,y} \\ \vdots & \ddots & \vdots & \ddots & \vdots \\ ma_{1,1} & \cdots & ma_{x,k} & \cdots & ma_{x,y} \end{bmatrix}_{X \times Y} \quad (1)$$

The preliminary Tasmanian devil population is signified as MA , and the j^{th} potential solution is signified as Ma_j . Likewise, the applicant valuation of the k^{th} value is defined as $Ma_{j,k}$, and the space, including the problems and factors y , is symbolized as X . The objective function is expressed in the following Equation (2).

$$Fit = \begin{bmatrix} Fit_1 \\ \vdots \\ Fit_j \\ \vdots \\ Fit_X \end{bmatrix}_{X \times 1} = \begin{bmatrix} Fit(Ma_1) \\ \vdots \\ Fit(Ma_j) \\ \vdots \\ Fit(Ma_X) \end{bmatrix}_{X \times 1} \quad (2)$$

where F represents the optimal solution and Fit_j represents the j^{th} candidate solution of the objective function [30].

Phase of exploration: The Tasmanian devil in the j^{th} position chooses carrion first from the neighborhood by estimation based on the choice of random conditions as expressed in Equation (3).

$$DB_j = Ma_i, \quad i \in \{1, 2, \dots, X | i \neq j\}, \quad j = 1, 2, \dots, X \quad (3)$$

The chosen carrion in the j^{th} Tasmanian devil is depicted by DB_j . The new place is dependent on the chosen carcasses in the search space. The new agent's updated place could be formulated as given in Equations (4) and (5).

$$ma_{j,k}^{new, R_1} = \begin{cases} ma_{j,k} + S.(D_{j,k} - I.m_{j,k}), & Gd_j < G_j \\ ma_{j,k} + S.(D_{j,k} - m_{j,k}), & Otherwise \end{cases} \quad (4)$$

$$Ma_j = \begin{cases} ma_{j,k}^{new, R_1}, & G_j^{new, R_1} < G_j \\ Ma_j, & Otherwise \end{cases} \quad (5)$$

Based on the initial strategic plan, the new and updated condition has been signified as $ma_{j,k}^{new, R_1}$. The absolute function and the arbitrary durations are both between 0 and 1, while the random number I is between 1 and 2 [31].

Phase of exploitation: Depending on the position of the predators, the same location of other Tasmanian devil populations can be assumed with the choice of prey as described by Equation (6).

$$P_j = Ma_i, \quad i \in \{1, 2, \dots, X | i \neq j\}, \quad j = 1, 2, \dots, X \quad (6)$$

When it discovers an improved result based on the objective function, it changes its current stance and decides on a new role as expressed by Equations (7) and (8).

$$ma_{j,k}^{new, R_2} = \begin{cases} ma_{j,k} + S.(a_{j,k} - I.m_{j,k}), & Gq_j < G_j \\ ma_{j,k} + S.(m_{j,k} - a_{j,k}), & Otherwise \end{cases} \quad (7)$$

$$M_j = \begin{cases} M_{j,k}^{new, R_2}, & G_j^{new, R_2} < G_j \\ M_j, & Otherwise \end{cases} \quad (8)$$

Considering the Devil chosen value as a target of predators and following the previous value, an optimal scheduling solution is established, and the procreation of the devil's place is approximated following Equations (9)–(11).

$$ma_{j,k}^{new} = ma_{j,k} + (2s - 1).s.ma_{j,k} \quad (9)$$

$$s = 0.01 \left(1 - \frac{1}{\text{maximum iteration}} \right) \quad (10)$$

$$Ma_j = \begin{cases} Ma_j^{new}, & G_j^{new} < G_j \\ Ma_j, & \text{Otherwise} \end{cases} \quad (11)$$

The current incarnation is portrayed as an *iteration*, while the total number of iterations is indicated as the *maximum iteration*. The most pertinent and low-dimensionality features are picked from the dataset attributes as a result of its new status, where the j^{th} Tasmanian devil of the neighbourhood is M_j^{new} and the fitness value is G_j .

3.3. Improved Grey Wolf Optimization Algorithm-Based Deep-CNN for Lung Cancer Detection

The IoT-enabled healthcare monitoring system allows the Improved Grey Wolf Optimization (IGWO) algorithm to fine-tune parameters for training via the Deep Convolutional Neural Network (DCNN) model, resulting in high detection efficiency of lung cancer. This section explores the IGWO's operating mechanism for parameter tuning and the IGWO-based DCNN model.

A. Improved Grey Wolf Optimization

The social leadership hierarchy and group hunting behaviour of GWO are improved in terms of convergence rate, resulting in the IGWO that determines the optimal solution in group β being placed at the top of the hierarchical pyramid to assist the rest of the group and the position of the prey as presented in Equation (12). The IGWO is then used to integrate data from the IoT-enabled healthcare system to fine-tune the settings for training through the DCNN for lung disease diagnosis.

$$M_r^{k(t)} = \left((W_\beta \times M_\beta^k(t)) + (W_\gamma \times M_\gamma^k(t)) + (W_\delta \times M_\delta^k(t)) \right) + \mu(t) \quad (12)$$

The solution to each d dimension issue can be represented as $k = 1, 2, \dots, d$ and the position of the prey can be evaluated for the k^{th} element at the t iteration and is represented as $F : M_r^k(t)$. The rigorous social leadership of the grey wolf pack and its weights can be represented as $W = (W_\beta, W_\gamma, W_\delta)$ and each weight should be between 0 and 1 such that their aggregate equals 1, as indicated by the inequality and equity criteria provided in Equations (13) and (14), respectively [32].

$$1 \geq W_\beta > W_\gamma > W_\delta \geq 0 \quad (13)$$

$$W_\beta + W_\gamma + W_\delta = 1 \quad (14)$$

The stochastic error can be evaluated as $\mu(t) \sim X(0, \sigma(t))$ [33], where the standard deviation and mean of the Gaussian distribution are stated as $\sigma(t)$ and $\mu(t)$. Consequently, we define the property of dynamic deviation as given in Equation (15) and thereby we update the location of the k^{th} wolf as represented by Equation (16). Eventually, at the k^{th} dimension at the t^{th} and j^{th} solutions are regarded as $M_{j(t)}^k$.

$$\sigma(t) > \sigma(t + 1) \quad (15)$$

$$M_r^k(t + 1) = M_r^k(t) - R \times \left| M_r^k(t) - M_{j(t)}^k \right| \quad (16)$$

The new local optimal is explored provided that $|R| > 1$ by employing the random (R) in the interval $[-2, 2]$ and the prey searching and attacking are implied utilizing the $|R| > 1$ and $|R| < 1$ conditions, respectively. The new position can be derived using Equation (5) outside the restriction, where the constraints are estimated by random steps, as shown in Equation (17).

$$M_r^k(t+1) = \begin{cases} M_r^k(t) + v \times (U^k - M_j^k(t)), & \text{if } M_j^k(t+1) > U^k \\ M_r^k(t) + v \times (L^k - M_j^k(t)), & \text{if } M_j^k(t+1) > L^k \end{cases} \quad (17)$$

where U^k and L^k indicate the upper and lower boundaries of the constraints, respectively, and V is an arbitrary value between 0 and 1. The wolf's random movements are considerably determined when executing the prey-finding process, as shown in the systematic flowchart of the standard GWO algorithm in Figure 2.

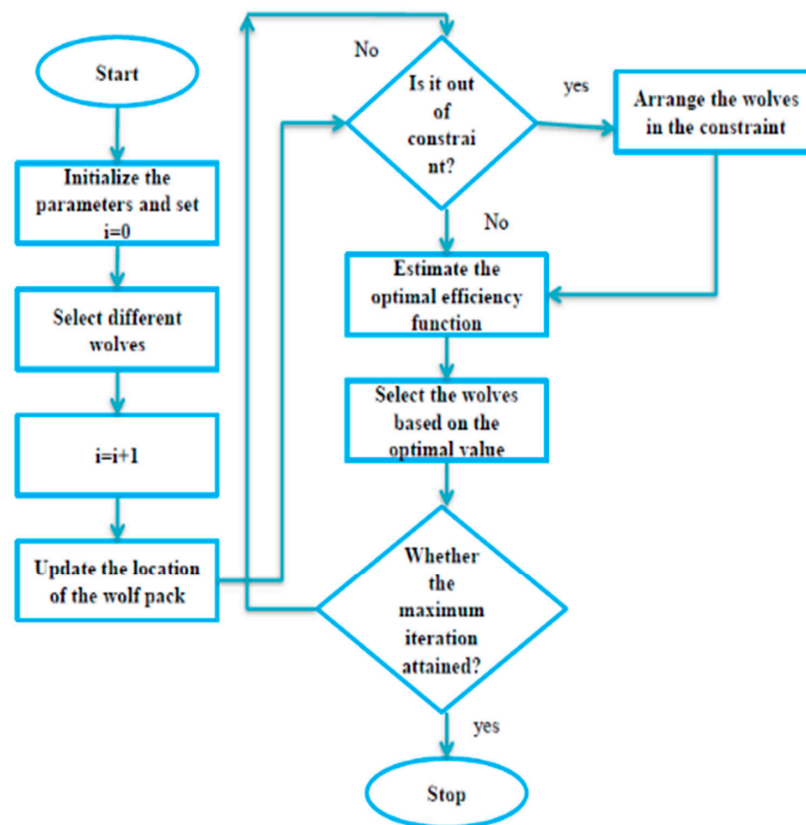


Figure 2. Systematic flowchart of the Grey Wolf Optimization algorithm for fine-tuning of the parameters.

Given that the GWO converges slowly, with a lower convergence rate at the early stage and a higher convergence rate at the latter stage [34,35], we updated the convergence rates at the early and later stages by integrating Equations (18) and (19), respectively.

$$h = 0.9 \times \left(2 - t \times \frac{2}{Max_iter} \right) \quad (18)$$

$$h = 1.2 \times \left(2 - t \times \frac{2}{Max_iter} \right) \quad (19)$$

where h is the convergence rate, t is the iteration index, and Max_iter is the total number of iterations. Likewise, to minimize the local optimal fall, we utilize sine-cosine functions

illustrated in Equation (20), and the resulting improved GWO algorithm is then employed to fine-tune the parameters for training through the DCNN for lung cancer diagnosis.

$$M_j^k(t+1) = \sin(t)M_1 + \sin(t)\cos(t)M_2 + \cos(t)M_3 \quad (20)$$

B. Improved grey wolf optimization algorithm-based deep convolution neural network model

The deep convolution neural network classifier configuration comprises several layers, each of which defines a combination of nodes and functionalities, as depicted in Figure 3. The convolution layer generates image features, while the classification strands generate the final output [36]. The DCNN classifier's input layer is initially applied utilizing feature vectors recorded from the lung cancer patients, and the feature maps are further reduced by employing convolutional filters in the deep convolution neural network model for lung cancer detection. The neurons between layers communicate with each other via configurable heaps with the gradient output, which can be mathematically characterized as demonstrated in Equation (21).

$$CV^{p+1} = CV^p + \sum_{f=0}^J \sum_{h=0}^J (We)_f \times (bi)_f \quad (21)$$

In the above equation, * denotes the convolution layer and CV^{p+1} signifies the repaired extracted features of the convolution layer, where the weight lifting of the convolution layer identified by $(we)_f$ and the bias denoted by $(bi)_f$ are optimally optimized utilizing IGWO algorithm [37].

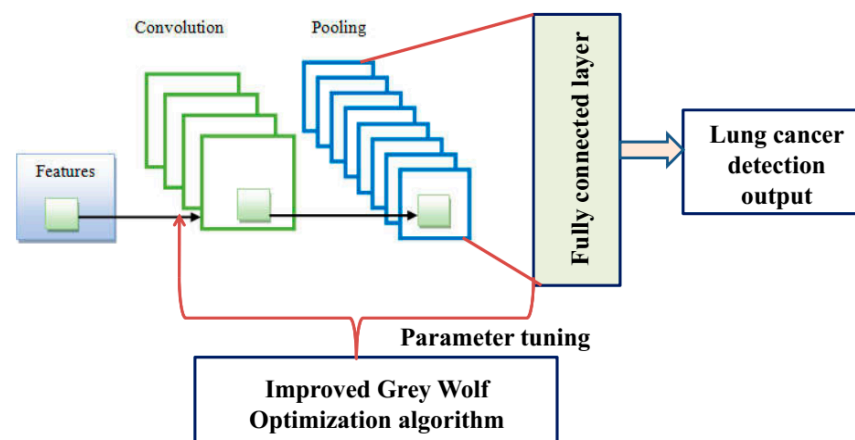


Figure 3. An illustration of integrating the improved grey wolf optimization algorithm to the deep convolution neural network for fine-tuning of the parameters.

The learning behaviour of the lung cancer detection model is improved by integrating a batch normalization layer between the convolution operation and the ReLU layer; as a result, this layer is accountable for regulating both the gradients and the authorizations in the system to ensure efficient training. The local information is transferred from the convolution layer to the quasi-ReLU layer, which has neither mass nor bias. Obtaining bottom-up samples from the returned features from the convolution layer within the max-pooling enables the reduction in information and geographic size. Depending on the preceding layer of the convolutional layer, the identical process of producing the finished piece within the fully connected layer is represented by Equations (22) and (23).

$$AR = X(CV^{p+1}) \quad (22)$$

$$C^{p+1} = CV^p + \sum_{f=0}^I \sum_{h=0}^I (CV)_f \times (Bias)_f \quad (23)$$

This implies that the suggested IGWO algorithm determines the weights of the training DCNN classifier for the optimum solution. Eventually, the output FC layer is regularized using the SoftMax activation function to facilitate efficient classification layer processing [38]. The categorization covering, which is the topmost layer of DCNN, applies the options generated by the SoftMax activation to each and all input data intended to check lung cancer for each selected feature vector [39,40]. Finally, the proposed IGWO-based DCNN model recognizes different stages of lung disorders such as asthma, chronic obstructive pulmonary disease (COPD), and normal.

4. Results and Discussion

This section describes the experimental setup, the dataset used, the results obtained, and the comparative outcomes in a broader context. The proposed IoT-based lung disease prediction healthcare monitoring system is built on the Android operating system and Python libraries.

4.1. Dataset Explanation

The proposed IGWO-based DCNN model is trained on the Exasens dataset [41], a lung diseases dataset with four types of respiratory diseases: asthma, chronic obstructive pulmonary disease (COPD) infected, and normal. The experimental results are incorporated on an NS-2 GPU-based computer with a16GB RAM and GTX1050 GPU as well as an Intel Core i5-8300H CPU trying to run TensorFlow 1.15. Belong to this dataset, 70% of data for training and rest of 30% data used for testing purpose. The optimized deep learning model is trained by adjusting the network configuration so that the modeling gets better over the course of training. The dataset, additionally, includes demographic data collected from sample saliva of four groups acquired from the Research Center Borstel, Bio Material Bank Nord (Borstel, Germany) following the samples collection regulations of the Luebeck University ethics committee [41].

4.2. Experimental Setup

The proposed work has been implemented with the incorporation of the microcontroller and other readily available hardware devices, coupled with the LoRa communication hardware that forwards the data to the cloud storage system. Different features such as the patient's age, chronic diseases, and gender have been saved and combined with the patient's ID in the suggested system. The data collection and processing are carried out on a Raspberry Pi single-board computer with the hardware configuration described in Table 2.

Table 2. The hardware and their configuration setup used in the experiment.

| Hardware | Explanation |
|-----------------|---|
| SX1272 | Act as transmitter and receiver with 900 MHz LoRa |
| AD8232 | The electrocardiographic board used in Analog Devices |
| User Computer | Inter® Core™ i5-2400CPU@3.10 GHz PC |
| Raspberry Pi-IV | 1.5 GHz quad-core 64-bit ARM Cortex-A72 CPU |

4.3. Performance Metrics

The proposed IGWO-based DCNN for lung disease is assessed using sensitivity, specificity, accuracy, precision, disease prevalence, and negative predictive value. The outcomes are evaluated against cutting-edge clinical decision support systems (CDSS) [20], regional-based convolutional neural networks (RCNN) [21], active contour method (ACM) [25],

and Mask Region-Convolutional Neural Networks (Mask R-CNN) [26]. For clarity, the performance measurements are discussed in more detail below.

(i) Sensitivity

The sensitivity evaluates the various methods by assessing the capacity of the anticipating based on the features acquired against the method's estimated outcomes, as indicated in Equation (24).

$$Sen = \frac{G_p}{G_p + H_f} \quad (24)$$

(ii) Specificity

The specificity describes the ratio of true negative values to the total number of false cases in the system, with values of 0.0 and 1.0 for the worst and best case scenarios, respectively, and numerically can be stated as shown in Equation (25).

$$Spe = \frac{G_f}{G_f + H_f} \quad (25)$$

(iii) Accuracy

The accuracy is measured as the proportion of properly classified predictions (points) to the total number of predictions between 0 and 1, and it relies on how the data is normalized for the algorithm, as given in Equation (26).

$$Acc = \frac{G_p + G_f}{G_p + G_f + H_f + H_p} \quad (26)$$

(iv) Precision (Negative Predict Value)

The precision measures the number of accurate positive predictions made by the algorithm, and it is determined mathematically as the ratio of properly predicted positive instances divided by the total number of positive examples anticipated, as provided in Equation (27).

$$Pre = \frac{G_p}{G_p + H_p} \quad (27)$$

(v) Disease Prevalence

The disease prevalence is the clinical prognosis that defines the likelihood of discovering the disease (i.e., lung disease) among patients before the screening test and can be expressed mathematically, as described in Equation (28).

$$DP = \frac{G_p + G_f}{G_p + G_f + H_f + H_p} \quad (28)$$

(vi) Negative Predict Value

The negative predictive value (NPV) is the proportion of patients with negative test results who are already healthy, and it is mathematically defined as the ratio of subjects properly classified as negative to all those with negative test findings (Equation (29)).

$$NPV = \frac{G_f}{G_f + H_p} \quad (29)$$

In the above Equations (28) and (29), the G_p represents the true positive, G_f denotes the true negative, H_p denotes the false positive, and H_f denotes the false negative, respectively.

4.4. Comparative Study

In this section, we contrast the proposed IGWO-based DCNN model's performance to that of the existing CDSS [20], RCNN [21], ACM [25], and Mask R-CNN [26] models while taking into account the aforementioned performance assessment criteria. In Figure 4, the sensitivity comparison analysis of the different lung disease-predicting models is presented. The graph indicates that employing the IGWO algorithm enhances the performance of the DCNN by attaining the highest sensitivity of 97.67%. Meanwhile, CDSS [20], RCNN [21], ACM [25], and Mask R-CNN [26] reach 90.21%, 89.67%, 95.34%, and 93.54%, respectively. The work's specificity is compared to comparable works and plotted in a graphical form, as seen in Figure 5. From the graph, it can be seen that the suggested work has a higher specificity of 98.12%, whereas other works have a lower proportion. The suggested IGWO expands search-ability and, as a result, expands the prediction of lung diseases and reduces inaccurate prediction.

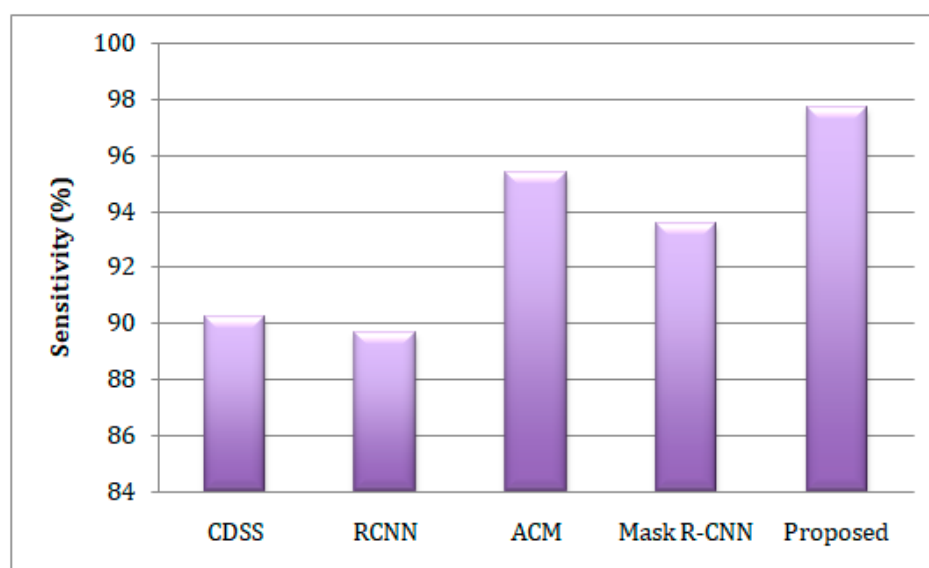


Figure 4. A comparison of the estimation of sensitivity corresponding to the different lung disease predictive models.

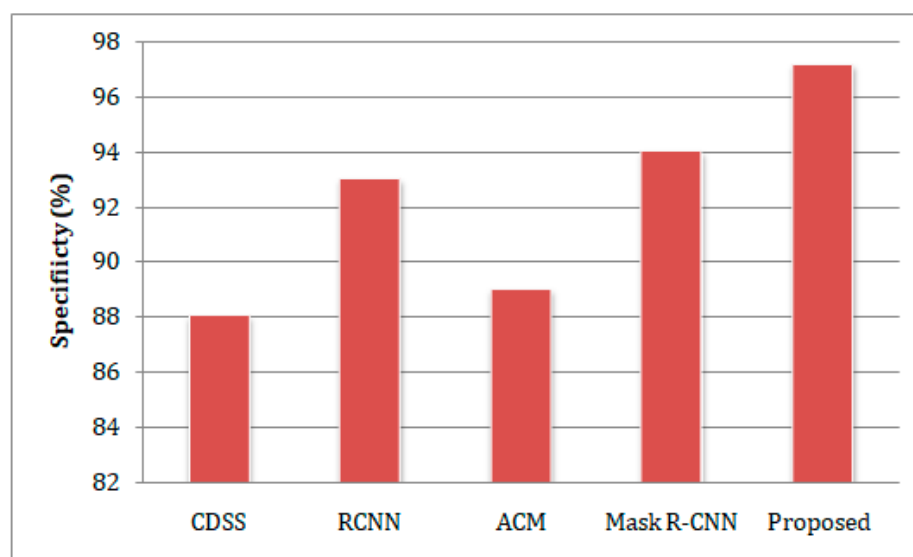


Figure 5. A comparison of the estimation of specificity concerning the different methods.

In comparison to existing methodologies, the presented study has greater prediction accuracy, as depicted in Figure 6. The lung disease prediction of our suggested health-care monitoring system reaches 98.27%, whereas the techniques CDSS [20], RCNN [21], ACM [25], and Mask R-CNN [26] show 91.78%, 95.26%, 92.89%, and 91.76%, respectively. Figure 7 shows the precision-based comparison analysis. When compared to the other methods, which only achieve low precision, our suggested strategy obtains a precision of 99.15%. The suggested work was followed by the RCNN and ACM, which achieved around 94.0% and 92.0% precision, respectively, compared to the CDSS and Mask-RCNN, which achieved 88.0% and 88.5% precision, respectively.

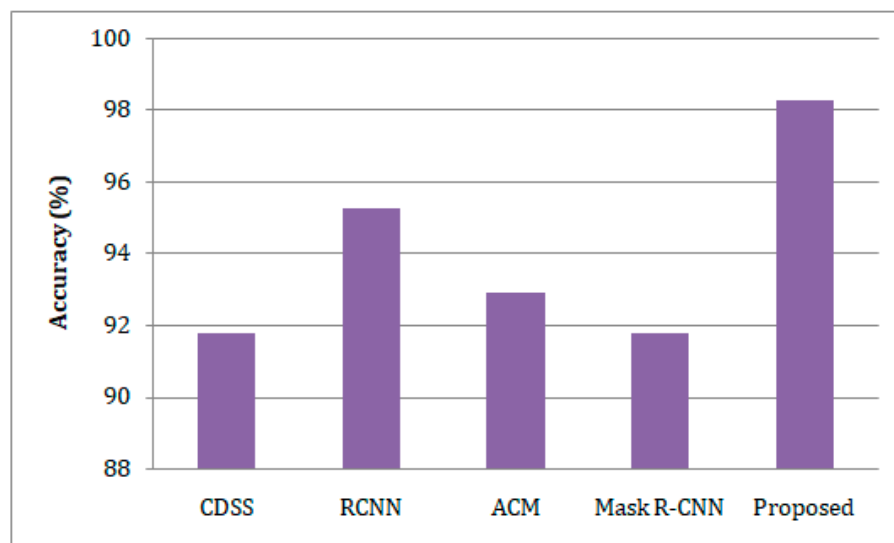


Figure 6. A comparison of the estimation of accuracy for lung disease with respect to the different predictive models.

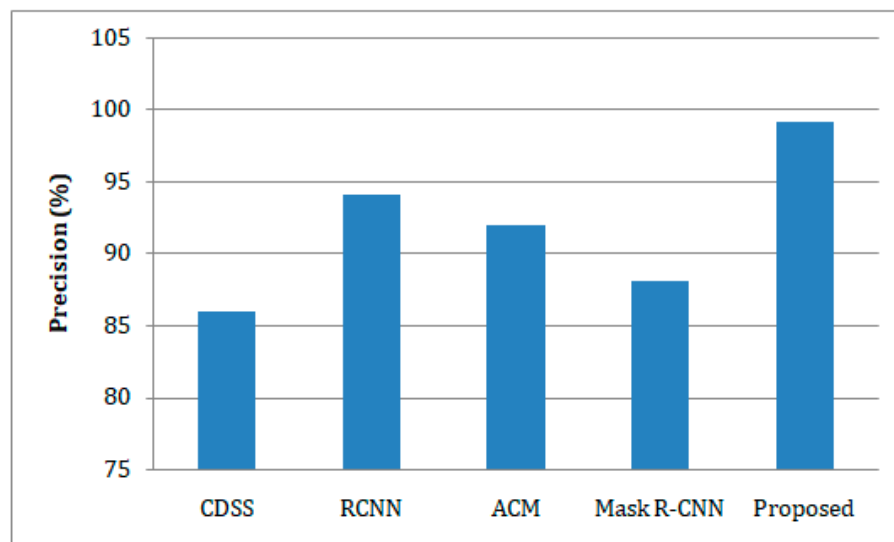


Figure 7. A comparison of the estimation of precision for lung disease with respect to the different predictive models.

The disease prevalence values and prediction values of the suggested and current techniques are compared in Tables 3 and 4 while taking into account the PPV and NPV values. It should be noted that the highest PPV value and vice versa have been attained when the disease prevalence is higher. In comparison to the DCSS, ACM, RCNN, and Mask-RCNN, the suggested IoT-enabled healthcare system outperforms with higher values

of the NPV and PPV. The PPV value of our suggested technique, for instance, is 99.78% when the records are equal to 5000, which indicates that lung disease is likely to occur following the screening test in this case. When evaluating 5000 records, however, the NPV value of our proposed strategy is 99.69%, which is greater than the other alternatives. Computational time analysis is depicted in Table 5. The time of Gray wolf optimization (GSO) is 8.1 s which is minimum to PSO and GA.

Table 3. Disease prevalence analysis based on positive predicted values (PPV).

| DP | Records | PPV(%) | | | | |
|-----|---------|--------|-------|-------|------------|----------|
| | | CDSS | RCNN | ACM | Mask R-CNN | Proposed |
| 67 | 567 | 86.56 | 89.90 | 91.23 | 94.46 | 98.87 |
| 79 | 895 | 92.65 | 91.67 | 95.45 | 93.36 | 99.23 |
| 100 | 1568 | 93.56 | 93.56 | 92.56 | 96.78 | 99.45 |
| 198 | 5000 | 94.34 | 94.89 | 93.66 | 97.78 | 99.78 |

Table 4. Disease prevalence analysis based on negative predicted values (NPV).

| DP | Records | NPV(%) | | | | |
|-----|---------|--------|-------|-------|------------|----------|
| | | CDSS | RCNN | ACM | Mask R-CNN | Proposed |
| 67 | 567 | 92.45 | 89.45 | 90.67 | 93.56 | 98.67 |
| 79 | 895 | 89.45 | 90.35 | 91.63 | 94.29 | 98.89 |
| 100 | 1568 | 91.98 | 91.56 | 92.40 | 95.78 | 99.45 |
| 198 | 5000 | 94.78 | 92.11 | 93.00 | 96.28 | 99.69 |

Table 5. Computational time analysis.

| Algorithms | Time in Seconds |
|-----------------------------------|-----------------|
| Particle swarm optimization (PSO) | 13 (s) |
| Genetic Algorithm (GA) | 10 (s) |
| Gray wolf optimization (GSO) | 8.1 (s) |

5. Conclusions

In this study, we introduced a novel IoT-enabled healthcare monitoring platform based on an Improve Grey Wolf Optimization (IGWO)-based deep convolutional neural network (DCNN) model. The fundamental mechanism of the Tasmanian Devil Optimization (TDO) algorithm for identifying the most relevant features for diagnosing lung disease is investigated. The standard GWO's convergence rate is modified, and the resulting improved GWO algorithm is used to fine-tune the parameters of the DCNN model. The suggested framework is developed using the Python DCNN libraries and the Android operating system, and it is tested by employing the Exasens benchmark dataset from the Research Center Borstel and the Bio Material Bank Nord (Borstel, Germany). The dataset consists of demographic data taken from saliva samples of four different groups, including those with asthma, chronic obstructive pulmonary disease (COPD), infection, and normal. Following the simulation outcomes, the suggested IGWO-based DCNN model outperform to the existing CDSS, RCNN, ACM, and Mask R-CNN models in terms of precision, accuracy, sensitivity, and specificity. In more detail, the suggested approaches have precision, accuracy, sensitivity, and specificity of 99.15%, 98.27%, 97.67%, and 98.12%, which are superior to the current CDSS, RCNN, ACM, and Mask R-CNN methods.

Author Contributions: Conceptualization, R.R.I.; methodology, R.R.I.; investigation, R.R.I.; writing—original draft preparation, R.R.I., S.H., S.S.S.; writing—review and editing, S.H., S.S.S., A.S.Z., D.Ø.M., A.A.A.; A.A.A.A.; K.A.A.N., O.A.S.A.; supervision, S.S.S., D.Ø.M.; project administration, R.R.I., D.Ø.M., A.A.A., A.A.A.A., K.A.A.N., O.A.S.A. All authors have read and agreed to the published version of the manuscript.

Funding: The authors are thankful to the Deanship of Scientific Research at Najran University for funding this work under the Research Groups Funding program grant code (NU/RG/SERC/11/4).

Institutional Review Board Statement: Not applicable.

Informed Consent Statement: Informed consent does not apply as this was a retrospective review with no identifying patient information. This article does not contain any studies with human or animal subjects performed by any of the authors.

Data Availability Statement: Not applicable.

Conflicts of Interest: The authors declare no conflict of interest.

References

1. Jemal, A.; Siegel, R.; Ward, E.; Hao, Y.; Xu, J.; Thun, M.J. Cancer statistics, 2009. *CA Cancer J. Clin.* **2009**, *59*, 225–249. [[CrossRef](#)] [[PubMed](#)]
2. Zhou, B.; Yang, X.; Zhang, X.; Curran, W.J.; Liu, T. Ultrasound elastography for lung disease assessment. *IEEE Trans. Ultrason. Ferroelectr. Freq. Control* **2020**, *67*, 2249–2257. [[CrossRef](#)] [[PubMed](#)]
3. Demir, F.; Sengur, A.; Bajaj, V. Convolutional neural networks-based efficient approach for classification of lung diseases. *Health Inf. Sci. Syst.* **2020**, *8*, 4. [[CrossRef](#)] [[PubMed](#)]
4. Ghosal, R.; Kloer, P.; Lewis, K.E. A review of novel biological tools used in screening for the early detection of lung cancer. *Postgrad. Med. J.* **2009**, *85*, 358–363. [[CrossRef](#)]
5. Feng, F.; Wu, Y.; Wu, Y.; Nie, G.; Ni, R. The effect of artificial neural network model combined with six tumor markers in auxiliary diagnosis of lung cancer. *J. Med. Syst.* **2012**, *36*, 2973–2980. [[CrossRef](#)] [[PubMed](#)]
6. Greenberg, A.K.; Lee, M.S. Biomarkers for lung cancer: Clinical uses. *Curr. Opin. Pulm. Med.* **2007**, *13*, 249–255. [[CrossRef](#)] [[PubMed](#)]
7. Ma, P.C.; Blaszkowsky, L.; Bharti, A.; Ladanyi, A.; Kraeft, S.K.; Bruno, A.; Salgia, R. Circulating tumor cells and serum tumor biomarkers in small cell lung cancer. *Anticancer Res.* **2003**, *23*, 49–62. [[PubMed](#)]
8. Chu, X.Y.; Hou, X.B.; Song, W.A.; Xue, Z.Q.; Wang, B.; Zhang, L.B. Diagnostic values of SCC, CEA, Cyfra21-1 and NSE for lung cancer in patients with suspicious pulmonary masses: A single center analysis. *Cancer Biol. Ther.* **2011**, *11*, 995–1000. [[CrossRef](#)]
9. Prakash, N.; Kumar, A.; Kumar, P. Neuron-specific enolase as a biomarker: Biochemical and clinical aspects. *Sensors* **2015**, *15*, 24375–24396. [[CrossRef](#)]
10. Park, S.; Ock, C.-Y.; Kim, H.; Pereira, S.; Park, S.; Ma, M.; Choi, S.; Kim, S.; Shin, S.; Aum, B.J.; et al. Artificial Intelligence-Powered Spatial Analysis of Tumor-Infiltrating Lymphocytes as Complementary Biomarker for Immune Checkpoint Inhibition in Non-Small-Cell Lung Cancer. *J. Clin. Oncol.* **2022**, *40*, 1916. [[CrossRef](#)]
11. Caron, J.; Mangé, A.; Guillot, B.; Solassol, J. Highly sensitive detection of melanoma based on serum proteomic profiling. *J. Cancer Res. Clin. Oncol.* **2009**, *135*, 1257–1264. [[CrossRef](#)] [[PubMed](#)]
12. Shafique, K.; Khawaja, B.A.; Sabir, F.; Qazi, S.; Mustaqim, M. Internet of things (IoT) for next-generation smart systems: A review of current challenges, future trends and prospects for emerging 5G-IoT scenarios. *IEEE Access* **2020**, *8*, 23022–23040. [[CrossRef](#)]
13. Booi, T.M.; Chiscop, I.; Meeuwissen, E.; Moustafa, N.; den Hartog, F.T. ToN_IoT: The Role of Heterogeneity and the Need for Standardization of Features and Attack Types in IoT Network Intrusion Data Sets. *IEEE Internet Things J.* **2021**, *9*, 485–496. [[CrossRef](#)]
14. Ratnaparkhi, S.; Khan, S.; Arya, C.; Khapre, S.; Singh, P.; Diwakar, M.; Shankar, A. Smart agriculture sensors in IOT: A review. *Mater. Today Proc.* **2020**. [[CrossRef](#)]
15. Alam, M.M.; Malik, H.; Khan, M.I.; Pardy, T.; Kuusik, A.; Le Moullec, Y. A survey on the roles of communication technologies in IoT-based personalized healthcare applications. *IEEE Access* **2018**, *6*, 36611–36631. [[CrossRef](#)]
16. Cai, Q.; Wang, H.; Li, Z.; Liu, X. A survey on multimodal data-driven smart healthcare systems: Approaches and applications. *IEEE Access* **2019**, *7*, 133583–133599. [[CrossRef](#)]
17. Wang, L. Deep Learning Techniques to Diagnose Lung Cancer. *Cancers* **2022**, *14*, 5569. [[CrossRef](#)]
18. Almezghwi, K.; Serte, S.; Al-Turjman, F. Convolutional neural networks for the classification of chest X-rays in the IoT era. *Multimed. Tools Appl.* **2021**, *80*, 29051–29065. [[CrossRef](#)]
19. Han, T.; Nunes, V.X.; Souza, L.F.D.F.; Marques, A.G.; Silva, I.C.L.; Junior, M.A.A.F.; Sun, J.; Reboucas Filho, P.P. Internet of medical things—Based on deep learning techniques for segmentation of lung and stroke regions in CT scans. *IEEE Access* **2020**, *8*, 71117–71135. [[CrossRef](#)]

20. Rehm, G.B.; Woo, S.H.; Chen, X.L.; Kuhn, B.T.; Cortes-Puch, I.; Anderson, N.R.; Adams, J.Y.; Chuah, C.N. Leveraging IoTs and machine learning for patient diagnosis and ventilation management in the intensive care unit. *IEEE Pervasive Comput.* **2020**, *19*, 68–78. [\[CrossRef\]](#)
21. Ahmed, I.; Ahmad, A.; Jeon, G. An IoT-based deep learning framework for early assessment of COVID-19. *IEEE Internet Things J.* **2020**, *8*, 15855–15862. [\[CrossRef\]](#) [\[PubMed\]](#)
22. Ma, F.; Yu, L.; Ye, L.; Yao, D.D.; Zhuang, W. Length-of-stay prediction for pediatric patients with respiratory diseases using decision tree methods. *IEEE J. Biomed. Health Inform.* **2020**, *24*, 2651–2662. [\[CrossRef\]](#)
23. Xu, Y.; Holanda, G.; Souza, L.F.D.F.; Silva, H.; Gomes, A.; Silva, I.; Ferreira, M.; Jia, C.; Han, T.; de Albuquerque, V.H.C.; et al. Deep learning-enhanced internet of medical things to analyze brain CT scans of hemorrhagic stroke patients: A new approach. *IEEE Sens. J.* **2020**, *21*, 24941–24951. [\[CrossRef\]](#)
24. Skourt, B.A.; El Hassani, A.; Majda, A. Lung CT image segmentation using deep neural networks. *Procedia Comput. Sci.* **2018**, *127*, 109–113. [\[CrossRef\]](#)
25. Medeiros, A.G.; Guimarães, M.T.; Peixoto, S.A.; Santos, L.D.O.; da Silva Barros, A.C.; Rebouças, E.D.S.; de Albuquerque, V.H.C.; Rebouças Filho, P.P. A new fast morphological geodesic active contour method for lung CT image segmentation. *Measurement* **2019**, *148*, 106687. [\[CrossRef\]](#)
26. Cai, L.; Long, T.; Dai, Y.; Huang, Y. Mask R-CNN-based detection and segmentation for pulmonary nodule 3D visualization diagnosis. *IEEE Access* **2020**, *8*, 44400–44409. [\[CrossRef\]](#)
27. Chaudhary, A.; Singh, S.S. Lung cancer detection on CT images by using image processing. In Proceedings of the 2012 International Conference on Computing Sciences, Phagwara, India, 14–15 September 2012; IEEE: Piscataway, NJ, USA, 2012; pp. 142–146.
28. Polat, K.; Güneş, S. Principles component analysis, fuzzy weighting pre-processing and artificial immune recognition system based diagnostic system for diagnosis of lung cancer. *Expert Syst. Appl.* **2008**, *34*, 214–221. [\[CrossRef\]](#)
29. Dehghani, M.; Hubálovský, Š.; Trojovský, P. Tasmanian Devil Optimization: A New Bio-Inspired Optimization Algorithm for Solving Optimization Algorithm. *IEEE Access* **2022**, *10*, 19599–19620. [\[CrossRef\]](#)
30. Kozakiewicz, C.P.; Ricci, L.; Patton, A.H.; Stahlke, A.R.; Hendricks, S.A.; Margres, M.J.; Ruiz-Aravena, M.; Hamilton, D.G.; Hamede, R.; McCallum, H. Comparative landscape genetics reveals differential effects of environment on host and pathogen genetic structure in *Tasmanian devils* (*Sarcophilus harrisii*) and their transmissible tumour. *Mol. Ecol.* **2020**, *29*, 3217–3233. [\[CrossRef\]](#) [\[PubMed\]](#)
31. McCallum, H.; Tompkins, D.M.; Jones, M.; Lachish, S.; Marvanek, S.; Lazenby, B.; Hocking, G.; Wiersma, J.; Hawkins, C.E. Distribution and impacts of Tasmanian devil facial tumor disease. *EcoHealth* **2007**, *4*, 318–325. [\[CrossRef\]](#)
32. Russell, T.; Lisovski, S.; Olsson, M.; Brown, G.; Spindler, R.; Lane, A.; Keeley, T.; Hibbard, C.; Hogg, C.J.; Thomas, F.; et al. MHC diversity and female age underpin reproductive success in an Australian icon; The Tasmanian Devil. *Sci. Rep.* **2018**, *8*, 4175. [\[CrossRef\]](#)
33. Sun, X.; Hu, C.; Lei, G.; Guo, Y.; Zhu, J. State feedback control for a PM hub motor based on gray wolf optimization algorithm. *IEEE Trans. Power Electron.* **2019**, *35*, 1136–1146. [\[CrossRef\]](#)
34. Novak, E. *Deterministic and Stochastic Error Bounds in Numerical Analysis*; Springer: Berlin/Heidelberg, Germany, 2006; Volume 1349.
35. Xie, Q.; Guo, Z.; Liu, D.; Chen, Z.; Shen, Z.; Wang, X. Optimization of heliostat field distribution based on improved Gray Wolf optimization algorithm. *Renew. Energy* **2021**, *176*, 447–458. [\[CrossRef\]](#)
36. Ren, A.; Li, Z.; Ding, C.; Qiu, Q.; Wang, Y.; Li, J.; Qian, X.; Yuan, B. Sc-dcn: Highly-scalable deep convolutional neural network using stochastic computing. *ACM Sigplan Not.* **2017**, *52*, 405–418. [\[CrossRef\]](#)
37. Jalali SM, J.; Ahmadian, S.; Khodayar, M.; Khosravi, A.; Shafie-khah, M.; Nahavandi, S.; Catalao, J.P. An advanced short-term wind power forecasting framework based on the optimized deep neural network models. *Int. J. Electr. Power Energy Syst.* **2022**, *141*, 108143. [\[CrossRef\]](#)
38. Jakhar, K.; Hooda, N. Big data deep learning framework using keras: A case study of pneumonia prediction. In Proceedings of the 2018 4th International Conference on Computing Communication and Automation (ICCCA), Greater Noida, India, 14–15 December 2018; IEEE: Piscataway, NJ, USA, 2018; pp. 1–5.
39. Ma, J.; Du, K.; Zheng, F.; Zhang, L.; Gong, Z.; Sun, Z. A recognition method for cucumber diseases using leaf symptom images based on deep convolutional neural network. *Comput. Electron. Agric.* **2018**, *154*, 18–24. [\[CrossRef\]](#)
40. Chakraborty, R.; Pramanik, A. DCNN-based prediction model for detection of age-related macular degeneration from color fundus images. *Med. Biol. Eng. Comput.* **2022**, *60*, 1431–1448. [\[CrossRef\]](#) [\[PubMed\]](#)
41. Available online: <https://www.kaggle.com/datasets/christopherwsmith/exasens-data-set> (accessed on 24 December 2022).

Disclaimer/Publisher’s Note: The statements, opinions and data contained in all publications are solely those of the individual author(s) and contributor(s) and not of MDPI and/or the editor(s). MDPI and/or the editor(s) disclaim responsibility for any injury to people or property resulting from any ideas, methods, instructions or products referred to in the content.